

Copyright © 2014, Paper 18-015; 58377 words, 9 Figures, 0 Animations, 2 Tables.  
<http://EarthInteractions.org>

# Validating ENSO Teleconnections on Southeastern U.S. Winter Hydrology

**Bappaditya Nag\***

Department of Earth, Ocean and Atmospheric Science, and Center for Ocean-Atmospheric Prediction Studies, Florida State University, Tallahassee, Florida

**V. Misra**

Department of Earth, Ocean and Atmospheric Science, and Center for Ocean-Atmospheric Prediction Studies, and Florida Climate Institute, Florida State University, Tallahassee, Florida

**S. Bastola**

Center for Ocean-Atmospheric Prediction Studies, Florida State University, Tallahassee, Florida, and School of Civil and Environmental Engineering, Georgia Institute of Technology, Atlanta, Georgia

Received 30 October 2013; accepted 10 June 2014

**ABSTRACT:** In this study, the authors contrast four century-long meteorological datasets comprising of two sets of observations [Climate Research Unit (CRU) and Parameter–Elevation Regressions on Independent Slopes Model (PRISM)] and two atmospheric reanalyses [Twentieth Century Reanalysis (20CR) and Florida Climate Institute–Florida State University Land–Atmosphere

---

\* Corresponding author address: Bappaditya Nag, Department of Earth, Ocean and Atmospheric Science, Florida State University, P.O. Box 3064520, Tallahassee, FL 32306-4520.  
E-mail address: [bnag@coaps.fsu.edu](mailto:bnag@coaps.fsu.edu)

Regional Reanalysis version 1.0 (FLAReS1.0)] to diagnose the El Niño–Southern Oscillation (ENSO) forced variations on the streamflow in 28 watersheds spread across the southeastern United States (SEUS). The datasets are used to force three different lumped (calibrated) hydrological models with precipitation from these four sources of century-long datasets separately to obtain the median prediction from 1800 (=3 models  $\times$  600 simulations per model per watershed per season) multimodel estimates of seasonal mean streamflow across the 28 watersheds in the SEUS for each winter season from 1906 to 2005. The authors then compare and contrast the mean streamflow and its variability estimates from all three of the century-long climate forcings. The multimodel strategy of simulating the seasonal mean streamflow is to reduce the hydrological model uncertainty. The authors focus on the boreal winter season when ENSO influence on the SEUS climate variations is well known.

The authors find that the atmospheric reanalysis over the SEUS is able to reasonably capture the ENSO teleconnections as depicted in the CRU and PRISM precipitation datasets. Even the observed decadal modulation of this teleconnection by Atlantic multidecadal oscillation (AMO) is broadly captured. The streamflow in the 28 watersheds also show similar consistency across the four datasets in that the positive correlations of the boreal winter Niño-3.4 SST anomalies with corresponding anomalies of streamflow, the associated shift in the probability density function of the streamflow with the change in phase of ENSO, and the decadal modulation of the ENSO teleconnection by the AMO are sustained in the streamflow simulations forced by all four climate datasets (CRU, PRISM, 20CR, and FLAReS1.0). However, the ENSO signal in the streamflow is consistently much stronger in the southern watersheds (over Florida) of the SEUS across all four climate datasets. During the negative phase of the AMO, however, there is a clear shift of the ENSO teleconnections with streamflow, with winter streamflows in northern watersheds (over the Carolinas) exhibiting much stronger correlations with the ENSO Niño-3.4 index relative to the southern watersheds of the SEUS. This study clearly indicates that the proposed methodology using FLAReS1.0 serves as a viable alternative to reconstruct twentieth-century SEUS seasonal winter hydrology that captures the interannual variations of ENSO and associated decadal variations forced by the AMO. However, it is found that the FLAReS1.0 forced streamflow is far from adequate in simulating the streamflow dynamics of the watershed over the SEUS at a daily time scale.

**KEYWORDS:** Winter/cool season; Hydrology

## 1. Introduction

Rapid demographic changes (Ting et al. 2009; Misra et al. 2011) along with prevalent robust climate variations (Ropelewski and Halpert 1986, 1987; Kiladis and Diaz 1989; Misra et al. 2009; Misra and DiNapoli 2012) in the southeastern United States (SEUS) pose a challenging task for managing freshwater resources. The impact of El Niño–Southern Oscillation (ENSO) on the climate of the SEUS and its modulation by the influence of low-frequency phenomena like the Atlantic multidecadal oscillation (AMO; Enfield et al. 2001; Tootle et al. 2005; Knight et al. 2006) and the Pacific decadal oscillation (PDO; Gershunov and Barnett 1998; Hidalgo and Dracup 2003) has been studied in some detail.

The importance of hydrologic data and their variability in planning and formulating policies for water resources management including irrigation,

environment flow, and reservoir management has resulted in growing interest in finding the link between hydrologic variability and natural climate variability such as ENSO phenomena (e.g., Zorn and Waylen 1997; Cayan et al. 1999; Poveda et al. 2001; Schmidt et al. 2001; Räsänen and Kumm 2012). Such teleconnections are widely exploited in making streamflow forecasts (e.g., Gutiérrez and Dracup 2001; Chiew et al. 2003; Tootle and Piechota 2004). For example, Gutiérrez and Dracup (2001) concluded that ENSO-based streamflow forecasts for reservoir and hydroelectric power distribution operation in Colombia was far superior over traditional streamflow forecasts that did not take ENSO into account. Such relationships are detectable in many regions with varying degrees of success including North America, where the correlation between peak season streamflow and ENSO are significantly persistent (Dettinger et al. 2000). Moreover, many studies report a contrasting strength of ENSO teleconnections over the Western Hemisphere between that in the recent decades and during the period from 1920 to 1950 (also Waylen et al. 1993; Räsänen and Kumm 2012). For instance, Schmidt et al. (2001) indicate that ENSO has a strong influence on rainfall and streamflow in the SEUS during the winter season. However, their study indicates that the response of streamflow to ENSO in the Florida Panhandle and south Florida is not uniform.

It is well known that warm (cold) ENSO events are characterized by colder and wetter (warmer and drier) boreal winter and spring seasons in the SEUS (Ropelewski and Halpert 1987; Kiladis and Diaz 1989). The magnitudes of these anomalies, however, decrease as one moves northward within the SEUS. In this study, further analysis is carried on the impacts of ENSO and its modulation by the low-frequency phenomena (AMO and PDO) on the rainfall and streamflow over several watersheds across the SEUS and their characterization in four different century-long precipitation datasets.

To achieve our objectives, we have examined the teleconnections from multiple datasets including those from independently analyzed rainfall observations and atmospheric reanalysis. The streamflow is estimated from multiple hydrological models (all of which are calibrated using an independent dataset of rainfall observations, which is not used in the intercomparison) to account for model uncertainty. Because of uncertainty in data, parameter, and structure of the hydrological model, the uncertainty in hydrological prediction is significant (Gupta et al. 2003; Beven 2005). Refsgaard et al. (2007) discuss methods to account for uncertainties in hydrological prediction. The generalized likelihood uncertainty estimation (GLUE) (Beven and Binley 1992) framework, a well-known method, is used in this study to account for uncertainties in hydrological simulation associated with the parameter and structure of the selected models (see Bastola et al. 2011).

The rest of the paper is organized as follows: The datasets used in the paper are described in section 2, followed by a description of the hydrological models in section 3. Section 4 discusses the results, and the concluding remarks are summarized in section 5.

## 2. Data

Two sets of atmospheric reanalysis [Twentieth Century Reanalysis (20CR; Compo et al. 2011) and Florida Climate Institute–Florida State University Land–Atmosphere Regional Reanalysis version 1.0 (FLAReS1.0; DiNapoli and Misra

2012; Misra et al. 2013)] and two independent rainfall observational datasets [viz., the Climate Research Unit (CRU; Mitchell and Jones 2005) and Parameter–Elevation Regressions on Independent Slopes Model (PRISM; Daly et al. 1994)] are used in the present study. The 20CR dataset has a spatial resolution of  $200\text{ km} \times 200\text{ km}$  and spans from 1871 to the present. The 20CR has several ensemble members. However, for this study we choose to pick one member of the ensemble. The FLAReS1.0 data are dynamically downscaled versions of such a member at 10-km grid resolution. Furthermore, dynamically downscaled datasets are a manifestation of nonlinear interactions of the small spatial scales and high-frequency variability, which is influenced by the large-scale lateral boundary forcing (Misra 2007; Misra et al. 2013). As shown in DiNapoli and Misra (2012) and Misra et al. (2013), such downscaled datasets can differ in important and significant manner from the large-scale reanalysis, especially at diurnal scales and even in removing artificial discontinuities prevalent in 20CR. Therefore, although FLAReS1.0 and 20CR are not totally independent datasets, they are still worth comparing. FLAReS1.0 was generated using the Regional Spectral Model (Kanamitsu et al. 2010) for downscaling. The FLAReS1.0 spans a period of 108 years from 1901 through 2008. Misra et al. (2013) indicate that, by dynamic downscaling 20CR, the artificial discontinuity observed in 20CR due to inhomogeneity in the density of observations around the 1940s is significantly reduced by the internal variations of the regional climate system in FLAReS1.0. Furthermore, DiNapoli and Misra (2012) and Misra et al. (2013) indicate that FLAReS1.0 simulates the decadal variations of winter precipitation, extreme events of winter freeze, precipitation associated with tropical cyclone landfall, and diurnal variations of precipitation with reasonable fidelity.

The CRU data are gridded rainfall observations (from rain gauge stations) available globally over land with a horizontal spacing of  $50\text{ km} \times 50\text{ km}$  and span a time period of 1901 through 2006 (Mitchell and Jones 2005). For the CRU data, reference series were constructed by using data from neighboring stations as proxy for grids with no observation stations. The station anomalies are interpolated to a 50-km grid and merged with the published 1961–90 series (Mitchell and Jones 2005). The PRISM dataset is another alternative rainfall observational dataset on a finer scale of 4-km grid resolution (Daly et al. 1994). Using a regression method, PRISM estimates the gridded precipitation from a point data source. The digital elevation model (DEM) is used to account for the effects of topography on precipitation. The PRISM data are available over only the continental United States. The domain of interest for our analysis in this paper is the SEUS:  $24^{\circ}$ – $37^{\circ}$ N,  $99^{\circ}$ – $75^{\circ}$ W. From all of the above-mentioned sources data were selected for a common period of 99 years at a monthly interval spanning from December 1906 through November 2005. For calibrating the hydrological models we made use of the unified daily U.S. precipitation analysis of the Climate Prediction Center (CPC) at 50-km grid resolution (Higgins et al. 2000), which is available from 1948 onward. Although CPC uses similar rain gauge observations as CRU and PRISM, they display some significant differences in their variations and seasonal mean (not shown) because of their varied gridding methodologies. We therefore regard the CPC rainfall dataset as pseudo-independent rainfall analysis data from CRU and PRISM, which are used in the calibration of the hydrological models. The CPC rainfall data make use of quality-controlled rain gauge data from a variety of sources—including the National Oceanic and Atmospheric Administration (NOAA)/National

Climate Data Center's (NCDC) daily co-op stations, river forecast centers data, and NCDC's hourly precipitation database—to generate this analyzed precipitation dataset. The CPC rainfall is available at daily interval unlike CRU and PRISM, which is available at monthly interval. However, to be consistent in our comparisons, rainfall from all sources was used at a monthly interval.

The extended reconstructed sea surface temperature, version 3 (ERSSTv3; [Smith and Reynolds 2004](#)), based on the International Comprehensive Ocean–Atmosphere Data Set (ICOADS) release 2.4, is used for the calculation of the Niño-3.4 SST seasonal anomaly index.

### 3. Hydrological model

Conceptual hydrological models are widely used to simulate hydrological response at watershed scales ([Bastola et al. 2011](#); [Kasiviswanathan et al. 2013](#); [Hughes 2013](#)). Such models use a range of simplifications to model a very complex and spatially distributed hydrological processes. Consequently, the process-based parameters of such models cannot be solely estimated based on their physical basis and must be estimated through model calibration. The experience of model calibration has defied the notion of existence of single set of best model parameters. The empirical evidence supporting the equifinality—that is, existence of a large model parameters set that results in equally acceptable model performance—is overwhelming ([Beven and Binley 1992](#); [Freer et al. 1996](#)). Therefore, in the past two decades uncertainty analysis has become an integral part of hydrological modeling. In this study, the uncertainty in hydrological models stemming from model parameters and model selection is accounted for by using three different models and a suite of their behavioral model parameters using the GLUE framework.

The hydrological simulation presented in this study builds on the work of [Bastola and Misra \(2013\)](#), who calibrated the hydrological models for watersheds of the SEUS using the GLUE framework. The brief outline of the method used is as follows:

- 1) Specify the range and distribution of model parameter. [Bastola and Misra \(2013\)](#) used uniform distribution from a specified range of values to define the prior distribution of model parameter.
- 2) Specify the likelihood measure [e.g., Nash–Sutcliffe efficiency (NSE)] and a threshold value (e.g.,  $NSE > 0.5$  as behavioral model parameter) to contrast behavioral from unbehavioral model parameters.
- 3) Retain the simulation from behavioral model parameter identified in step 2 and rank and produce likelihood-weighted model output.

In this study, the 600 behavioral model parameters for the selected watershed and hydrological model are taken from [Bastola and Misra \(2013\)](#). The behavioral model parameters were selected based on the NSE as a likelihood function. For the simulation of the streamflow in this paper, all 600 behavioral model parameters for each of the three models are used in this study within in the GLUE framework to account for uncertainties associated with the hydrological simulation. The multi-model estimate of the seasonal mean streamflow is then computed as the median of the 1800 simulations (=600 simulations per watershed per model  $\times$  3 hydrological models) per season. The models used in this study are the Hydrological Model (HyMOD; [Wagener et al. 2001](#); [Boyle et al. 2001](#)), the Nedbør-Afstrømnings model

(NAM; Madsen 2000), and the Tank model (Sugawara 1995). The HyMOD accounts for two different components in the hydrology of the watersheds. The fast component comprises surface processes like runoff while the slower component comprises subsoil processes like infiltration and interflow. Hence, the HyMOD uses a nonlinear tank connected to two tanks, each parameterizing the two processes of different rates. NAM (Madsen 2000) uses the base flow as a separate component and the surface and the interflow as a separate component in the simulation of the streamflow. The water content in different yet interconnected storages like surface zone storage, root-zone storage, and groundwater storage is accounted for in NAM model (Madsen 2000) to simulate different component of the hydrological cycle. The Tank model uses four tanks arranged vertically in series, each pertaining to model a specific process like surface runoff, intermediate runoff, subsurface runoff, and base flow (Sugawara 1995). These models are standard tools frequently used in hydrological studies. The parameters of these models are usually estimated through model calibration where the difference between model simulated value and observations are minimized with respect to some objective criteria: for example, Nash–Sutcliffe efficiency [Equation (1)] and volume error [VE; Equation (2)],

$$\text{NSE} = 1 - \frac{\sum_{i=1}^n (Q_i - Q_{\text{obs},i})^2}{\sum_{i=1}^n (Q_i - \overline{Q_{\text{obs}}})^2} \quad \text{and} \quad (1)$$

$$\text{VE} = \frac{\sum_{i=1}^n (Q_i - Q_{\text{obs},i})}{\overline{Q_{\text{obs}}}}, \quad (2)$$

where  $Q_i$  and  $Q_{\text{obs},i}$  are the simulated and the observed flow and  $n$  is the total number of points.

The time step used for all three hydrological models is daily. As the four dataset used in this study are monthly dataset, the weather generator is used to disaggregate a monthly total to produce a daily sequence of rainfall. In this study, the weather generator (WGEN) model following Richardson and Wright (1984) is used. Readers are referred to Wilks and Wilby (1999) for a review of weather generators. The WGEN uses a first-order Markov model to simulate the wet/dry day status, and it uses a two-parameter gamma distribution to model the precipitation amount in wet days. Use of WGEN to generate a daily rainfall sequence involves four parameters: that is, probability of a wet day following a wet day; a wet day following a dry day; and two parameters related to gamma distribution that synthesize the distribution of rainfall amounts, which are usually estimated from historical data. These four parameters for each of the selected watersheds were derived on the basis of 30 years of historical data (1948–77). Subsequently, these parameters are scaled on the basis of a monthly rainfall total to produce a daily rainfall sequence from 1905 to 2005. To scale the parameter of WGEN, the method outlined by Wilks (1992), which is based on a monthly change in mean and variance of rainfall,

is used. To scale the parameters, the change factor [Equation (3)] in precipitation is first derived for each month,

$$CF_{i,j,k} = \frac{(P_{i,j,k} - \overline{P_{j,k}})}{\overline{P_{j,k}}}, \quad (3)$$

where  $CF_{i,j,k}$  is the change factor for precipitation (e.g., for CRU precipitation) for the  $i$ th year,  $j$ th month, and  $k$ th watershed and  $\overline{P_{j,k}}$  is the climatologically average precipitation for the  $j$ th month and  $k$ th watershed derived from historical rainfall data from 1948 to 1977. Disaggregation of rainfall data from a monthly to daily time scale is done by scaling the parameter of the weather generator. As noted earlier, WGEN requires the specification of four parameters—namely, shape and scale parameters of the two-parameter gamma distribution parameters related to the probability of a wet day following a wet day and the probability of a dry day following a dry day—to model the sequence of rain and no rain events. Therefore, adapting these parameters to account for future changes requires four constraints to solve for the four parameters. One of the constraints is derived from a change in the mean value of rainfall and the remaining three constraints are relaxed through assumptions: that is, the probability of a wet day following a wet day and the probability of a dry day following a dry day are assumed constant and the change in variability of rainfall is assumed proportional to change in the mean (see Wilks 1992).

Calculations of the different metrics involved (e.g., correlations and composites) are done in the native grid of the datasets. The results of the analysis are tested for statistical significance using the bootstrapping method (McClave and Dietrich 1994; Efron and Tibshirani 1993). The idea of the bootstrapping is to create subsamples of the exact same size as the original dataset to form a distribution of the metric to be tested (e.g., correlation, composite anomalies). The concept of bootstrapping, which is a nonparametric test, tests the significance of a given metric against the null hypothesis that the quantitative value of the given metric can arise from a random distribution of the time series. For example, when we test for the significance of the correlations (see below; Figures 4, 5, 8, and 9) to the ENSO index, we compare the correlations therein to the distribution of the correlations obtained from 100 000 subsampled pairs of time series of the ENSO index with, say, a streamflow for a given watershed. These 100 000 pairs of time series have been obtained by randomly shuffling the (99) years of the original data of the ENSO Niño-3.4 index and streamflow for a given watershed. The correlations (e.g., in Figure 5) are then compared with this distribution of correlations obtained from the subsampled, randomly shuffled time series. If the sample correlation (e.g., Figure 5 below) is in either tail end of the distribution, then it is regarded to be statistically significant and the null hypothesis that the sample correlations can be randomly obtained is dismissed. So, when the correlations reside in the regions of lesser than the 5th percentile or greater than the 95th percentile (e.g., Figure 5), it is recognized as a statistically significant correlation at 10% significance level (denoted by the circles outlined with thick lines).

**Table 1. List of watersheds used in the study.**

Serial No.	Station	Lon (°W)	Lat (°N)	Station name
1	2456500	86.9833	33.7097	Locust Fork at Sayre, AL
2	3574500	86.3064	34.6242	Paint Rock River near Woodville, AL
3	2296750	85.5608	33.1167	Tallapoosa River at Wadley, AL
4	2329000	81.8761	27.2219	Peace River at Arcadia, FL
5	2365500	84.3842	30.5539	Ochlockonee River near Havana, FL
6	2375500	85.828	30.776	Choctawhatchee River at Caryville, FL
7	2236000	87.2342	30.965	Escambia River near Century, FL
8	2192000	81.3828	29.0081	St. Johns River near Deland, FL
9	2202500	82.77	33.9742	Broad River near Bell, GA
10	2217500	81.4161	32.1914	Ogeechee River near Eden, GA
11	2347500	83.4228	33.9467	Middle Oconee River near Athens, GA
12	2383500	84.2325	32.7214	Flint River near Culloden, GA
13	2339500	84.8331	34.5642	Coosawattee River near Pine Chapel, GA
14	2387000	85.1822	32.8861	Chatahoochee River at West Point, GA
15	2387500	84.928	34.667	Conasauga River at Tilton, GA
16	2102000	84.9414	34.5783	Oostanaula River at Resaca, GA
17	2118000	79.1161	35.6272	Deep River at Moncure, NC
18	2126000	80.659	35.845	South Yadkin River near Mocksville, NC
19	2138500	80.1758	35.1483	Rocky River near Norwood, NC
20	3443000	81.8903	35.7947	Linville River near Nebo, NC
21	3451500	82.624	35.299	French Broad River at Blantyre, NC
22	3504000	82.5786	35.6092	French Broad River at Asheville, NC
23	3512000	83.6192	35.1269	Nantahala River near Rainbow Springs, NC
24	3550000	83.3536	35.4614	Oconaluftee River at Birdtown, NC
25	2156500	83.9806	35.1389	Valley River at Tomotla, NC
26	2165000	81.4222	34.5961	Broad River near Carlisle, SC
27	2414500	82.1764	34.4444	Reedy River near Ware Shoals, SC
28	3455000	83.161	35.982	French Broad River near Newport, TN

## 4. Results

In this study, the impact of ENSO and decadal variations (e.g., AMO and PDO) on the winter rainfall and streamflow over 28 watersheds spread out in the SEUS is studied. The choice of these 28 watersheds follows from [Bastola and Misra \(2013\)](#). The watersheds are located in the states of Florida, Alabama, Georgia, and the Carolinas. These watersheds are a subset of the Model Parameter Estimation Experiment (MOPEX) U.S. watershed database ([Schaake et al. 2006](#); [Duan et al. 2006](#)). The name of the river basin, its U.S. Geological Survey (USGS) ID, and the location of the selected river gauging station are shown in [Table 1](#).

### 4.1. Fidelity of streamflow in the models

Before proceeding into the analysis of the streamflow, an assessment of the hydrological models would be useful. Two indices that are often used for the evaluation purpose are defined in [section 2](#): namely, Nash–Sutcliffe efficiency (NSE) index and volume error (VE). The NSE and VE were calculated for the winter streamflows simulated with 20CR and FLARes1.0 and validated against the corresponding simulated streamflow forced by the observed rainfall of CRU (left column) and that of the PRISM simulated flow (right column). These indices are

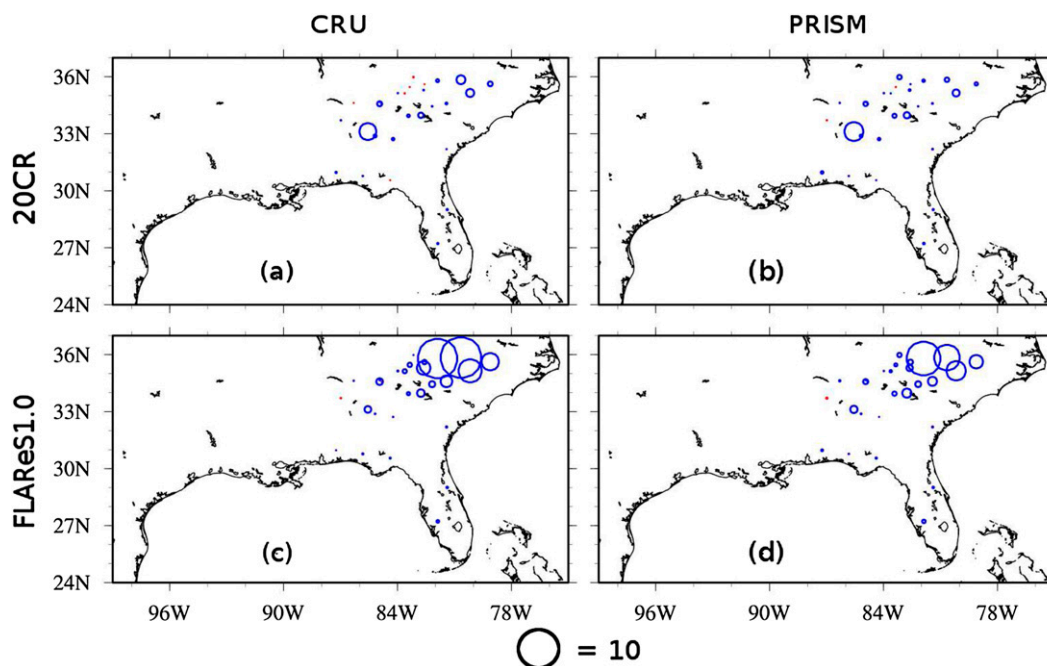


Figure 1. Nash-Sutcliffe error for (a),(b) 20CR and (c),(d) FLARes1.0 based on (a),(c) CRU and (b),(d) PRISM. Positive values are shown in red and negative values are shown in blue.

based on 99 years of flow. The NSE, as defined in Equation (1), is plotted for all the watersheds in Figure 1 and the VE is plotted in Figure 2. These values are also listed for individual watersheds in Table 2. Figure 3 gives a quantitative summary of both (Figures 1a,c and 2a,c). According to the definition, an ideal simulation will have an NSE value of 1 and a VE of 0. The NSE for most of the watersheds in the southern parts of the SEUS (Alabama, Florida, and parts of Georgia) is close to zero (Figures 1–3 and Table 2), while in the northern watersheds it is negative (Figures 1 and 2). The two atmospheric analyses (20CR and FLARes1.0) display a large negative NSE compared to the simulated flow forced by either CRU or PRISM. However, watersheds that have greater negative values of NSE overlay the regions where the precipitation is insignificantly correlated with ENSO and so are of lesser concern. VE is actually a fractional bias with lower values anticipated for good hydrological simulation. Northern watersheds in the Carolinas, northern Georgia, and northern Alabama display some of the largest VEs (Figure 2) in both reanalyses. In fact, parts of Florida, southern Alabama, and southern Georgia have a lower VE (Figures 2 and 3). A large fraction of the 28 watersheds in Figure 3 show that, for most of the river basins, the VE is clustered around 0–0.6 and the NSE is mostly clustered around 0 (Figure 3 and Table 2). It may be noted that 20CR has reduced variance in rainfall compared to FLARes1.0 (not shown), which results in reduced variance in the corresponding streamflow from 20CR, which produces higher NSE and lower VE scores than in FLARes1.0 (Figures 2 and 3).

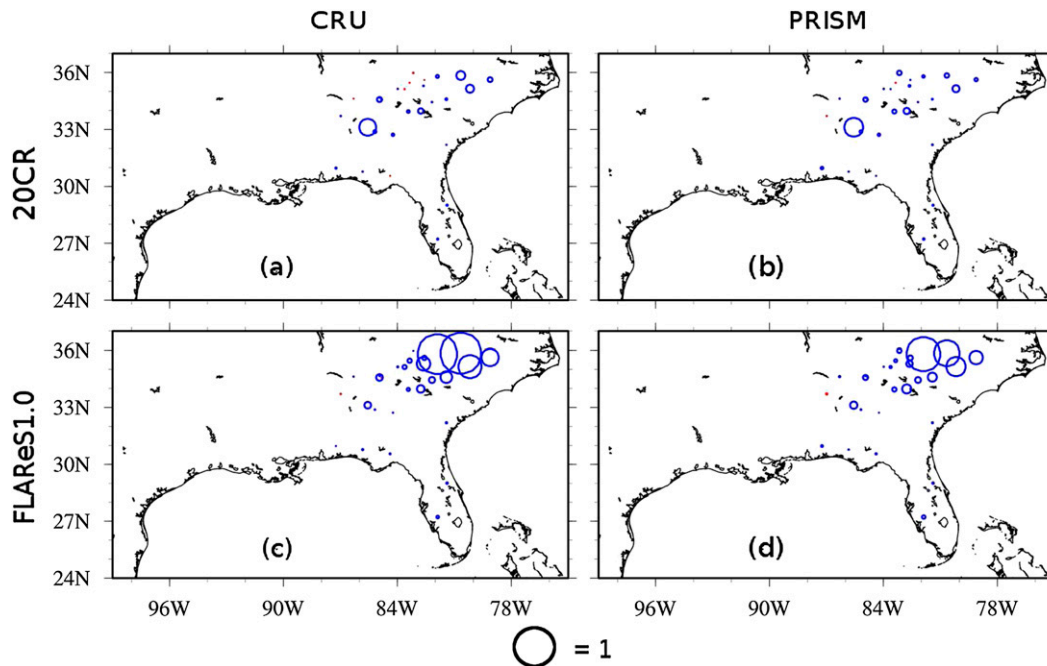


Figure 2. Volume error for (a),(b) 20CR and (c),(d) FLARes1.0 based on (a),(c) CRU and (b),(d) PRISM. Positive values are shown in red and negative values are shown in blue.

#### 4.2. The ENSO teleconnection

To get an overview of the influence of the different phases of the ENSO on the SEUS, a correlation for the regional precipitation with the Niño-3.4 SST seasonal mean index for winter seasonal mean [December–February (DJF)] rainfall anomalies is shown in Figure 4. The seasonal mean Niño-3.4 SST index anomalies are calculated by removing the 99-yr mean instead of a method adopted by CPC where a centered 30-yr mean is updated every 5 years. There are two reasons for removing a 99-yr mean instead of method adopted by CPC. First, the CPC provides indices dating back only to 1950. Second, this alternative definition of ENSO removes the confusion of calculation of the centered mean in the most recent 15 years of computation. The ENSO classification based on this definition of the Niño-3.4 SST seasonal anomaly index instead of that by the CPC lead to negligible differences. When tallied with the data provided by CPC from 1950 through 2005, only 4 years (1953, 1959, 1984, and 2005) out of 55 years turns out to be neutral years as per the definition used here, which otherwise is labeled as an El Niño or a La Niña year. With this classification, there are 28 El Niño, 26 La Niña, and 45 neutral years. The moderation of an ENSO event to a neutral event by this definition actually turns out to pose more strict limits to attain statistical significance of the results to detect ENSO teleconnections. It is important to point out that all the correlations (reported in the subsequent section) were carried out with respect to the seasonal anomaly

**Table 2. The Nash–Sutcliffe error and volume error for all SEUS watersheds (listed in Table 1) from simulated winter season streamflow forced by 20CR and FLAReS1.0 and validated against simulated streamflow forced by CRU and PRISM.**

Serial No.	20CR based on CRU		FLAReS1.0 based on CRU		20CR based on PRISM		FLAReS1.0 based on PRISM	
	NSE	VE	NSE	VE	NSE	VE	NSE	VE
1	-0.1725	0.3946	0.1547	0.2880	0.1139	0.2831	0.3362	0.1851
2	0.0279	0.2256	-0.1315	0.2828	-0.1399	0.2444	-0.3494	0.3026
3	-4.3830	0.9240	-1.7180	0.4216	-4.9002	0.9700	-1.8897	0.4556
4	-0.3330	0.2131	-0.6778	0.2946	-0.4225	0.2575	-0.8955	0.3420
5	0.0354	-0.0564	-0.2785	-0.0736	-0.0683	0.0311	-0.3438	0.0123
6	-0.1491	0.0126	-0.3170	-0.0301	-0.1235	0.0385	-0.1570	-0.0052
7	-0.3418	0.0641	-0.0596	-0.0419	-0.6563	0.1404	-0.4716	0.0268
8	-0.3415	0.2696	-0.4076	0.1824	-0.3224	0.2876	-0.4196	0.1992
9	-1.3809	0.4501	-1.9669	0.5458	-1.6114	0.4976	-2.3619	0.5965
10	-0.1000	0.2864	-0.3475	0.1977	-0.2313	0.3309	-0.2908	0.2391
11	-0.6886	0.4137	-0.7884	0.4042	-1.0518	0.4278	-1.1047	0.4182
12	-0.6318	0.4828	-0.1237	0.1458	-0.6341	0.4402	-0.0403	0.1129
13	-0.1891	0.2706	0.0407	0.1894	-0.1332	0.2110	-0.0393	0.1336
14	-0.7540	0.4052	-0.1859	0.2006	-0.6869	0.3644	-0.2306	0.1658
15	-0.0128	0.2346	-0.2289	0.2256	-0.1092	0.2145	-0.2388	0.2056
16	-1.2800	0.4869	-1.7059	0.5143	-1.1349	0.3705	-1.2969	0.3958
17	-1.2274	0.4021	-4.4855	0.8549	-0.8333	0.3310	-3.4920	0.7610
18	-2.2922	0.5336	-10.2719	1.2527	-1.1491	0.3502	-6.6526	0.9833
19	-2.0774	0.3472	-6.0056	0.6424	-1.8183	0.3023	-5.0118	0.5877
20	-0.7503	0.1833	-10.2719	0.9185	-0.6357	0.0785	-8.7930	0.7487
21	-0.2089	-0.0145	-3.5209	0.4993	-0.4566	-0.2309	-1.6428	0.1700
22	0.0073	0.0756	-1.1184	0.2571	-0.0859	0.1377	-1.2725	0.3298
23	0.1152	-0.0103	-1.0533	0.2044	-0.0773	-0.2337	-0.5800	-0.0674
24	0.0567	0.0776	-1.1036	0.2589	0.0850	-0.0202	-0.7778	0.1446
25	-0.1314	0.0173	-0.2783	-0.0806	-0.1647	0.0016	-0.1371	-0.0948
26	-0.4682	0.2781	-3.0278	0.7770	-0.2529	0.2052	-2.3383	0.6756
27	-0.1944	0.2426	-1.5620	0.4891	-0.1290	0.2237	-1.4988	0.4664
28	0.1854	0.2086	-0.0506	0.2118	-1.1613	0.4890	-1.1157	0.4929

Niño-3.4 index for the winter as the ENSO has a seasonal peak in the boreal winter months.

The correlations between the DJF precipitation from reanalysis and observations with the winter seasonal mean Niño-3.4 SST index indicate a positive correlation band over most parts of Florida and the southern parts of Alabama, Georgia, and South Carolina (Figure 4). In comparison to the correlations with the observed rainfall (Figures 4a,b), the 20CR dataset (Figure 4c) captures the ENSO teleconnection with rainfall over Florida quite well but does a comparatively poor job in representing this teleconnection in the other four states of our SEUS domain (Alabama, Georgia, and the Carolinas). FLAReS1.0 (Figure 4d) too displays a similar feature as 20CR with the ENSO teleconnections prevalent over Florida while it is relatively weak in the northern states of the SEUS. It should be noted that both CRU (Figure 4a) and PRISM (Figure 4b) display similar ENSO teleconnections, with positive correlations being strongest over peninsular Florida and slightly weaker but statistically significant positive correlations appearing along the coast from the Carolinas to the southern tier of states up to Texas.

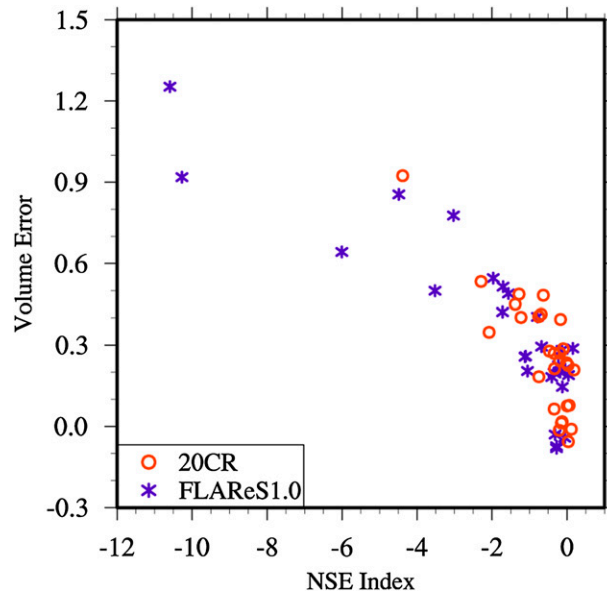


Figure 3. NSE index and volume error estimated based on CRU as reference data.

The six watersheds in the SEUS—two in Florida (Peace River and the St. John’s River basins), two in Alabama (Choctawhatchee River and Escambia River basins), and two in Georgia (Ogeechee River and Ochlockonee River basins)—can be expected to maintain these observed ENSO-forced atmospheric teleconnections in their streamflow since they lie in the region of strongest correlation of the precipitation with ENSO (Figure 4). It should be noted that some of the watersheds that spread across the states of Alabama and Georgia have their outlets in Florida where the streamflow is measured. Such watersheds will have their streamflow likely more influenced by the rainfall anomalies in Alabama and Georgia rather than that over Florida.

The correlation of the resulting winter seasonal mean streamflow with the corresponding Niño-3.4 SST index is shown in Figure 5. The CRU rainfall forced streamflow captures the positive correlation in the southern region of the SEUS and negative correlation higher up in the northern portion of the SEUS (Figure 5a). The results from PRISM (Figure 5b) compare well with the results from CRU (Figure 5a), especially for the southern watersheds in the domain. The 20CR (Figure 5c) captures the ENSO signal in Florida and Alabama but fails to capture more of the signal farther north, as depicted in Figures 5a,b. However, most of the watersheds located in the northern portion of the SEUS do not show any statistically significant correlation in either the observed or the reanalysis-forced rainfall datasets.

In fact, in contrast to Figure 4, the ENSO teleconnections of the streamflow in Figure 5 display many inconsistencies between the four datasets. For example the strength of the correlations in south Florida in CRU (Figure 5a) and PRISM (Figure 5b) are different. Likewise, the strength of the correlations over the southern watersheds differs between the reanalysis ENSO-forced streamflow variations (Figures 5c,d). A reason for this diversity in the streamflow response to ENSO could be

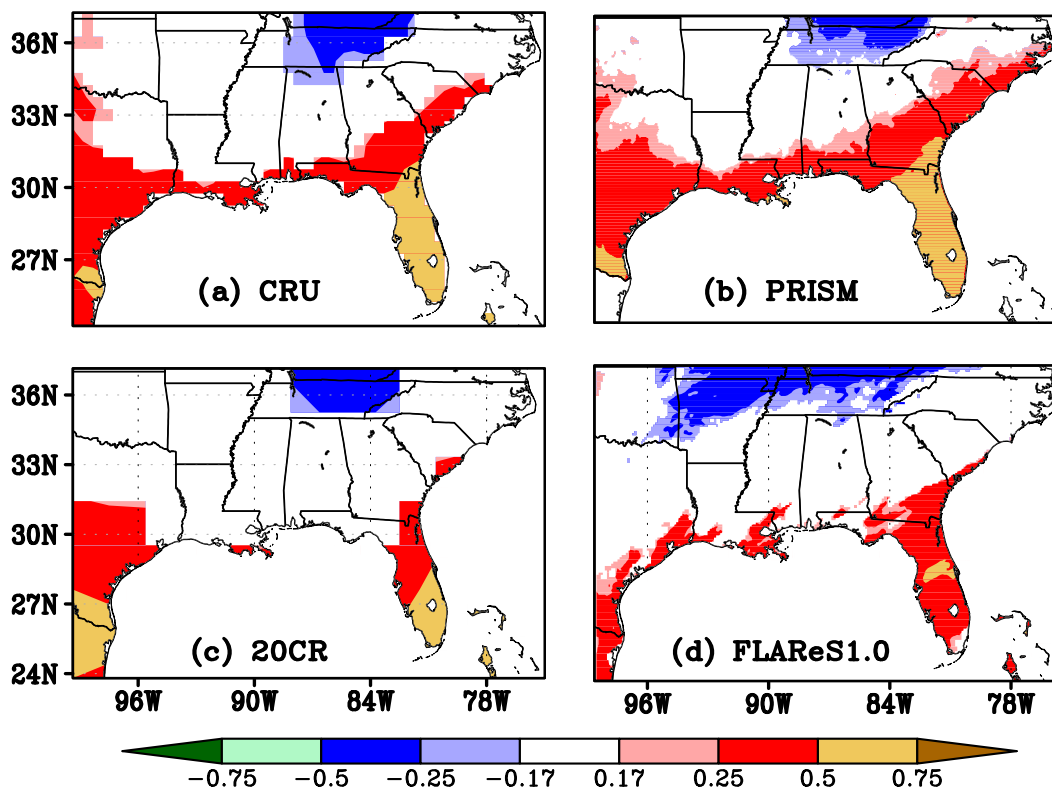
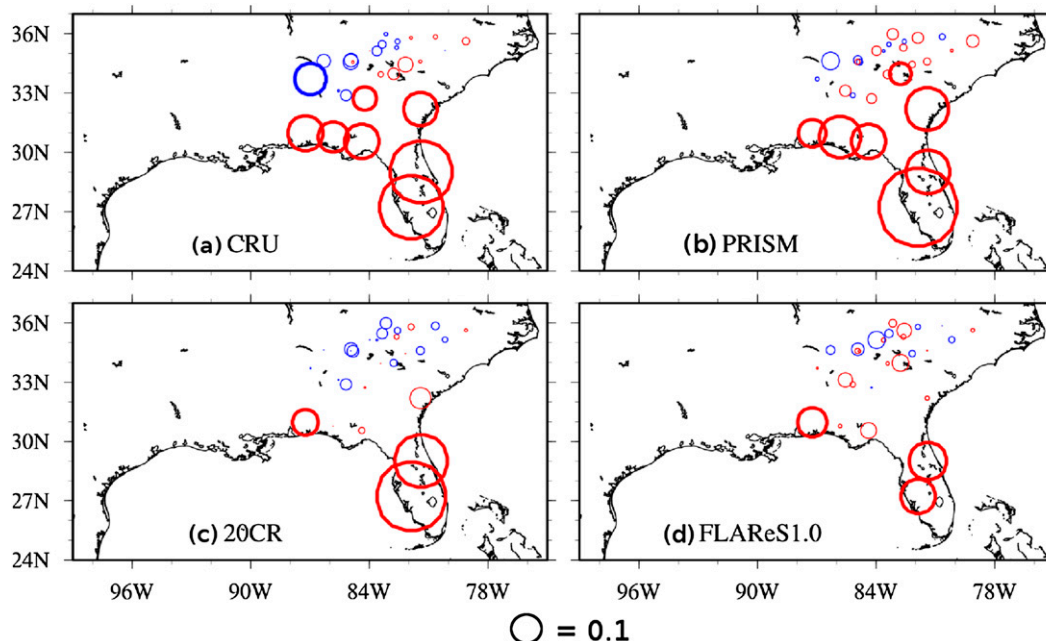


Figure 4. Correlation of DJF precipitation with Niño-3.4 index in (a) CRU, (b) PRISM, (c) 20CR, and (d) FLARes1.0. Statistically significant regions at the 90% level of confidence are shaded.

due to the fact that the relation between precipitation and streamflow is not linear in these watersheds (Oh and Sankarasubramanian 2012). Many of the watersheds in the middle and northern part of the SEUS domain fall in the region where the rainfall is insignificantly correlated with ENSO or the watersheds spans a region of diverse ENSO teleconnections (positive and negative correlations with ENSO index). In a related study, Sankarasubramanian et al. (2001) showed that the streamflow in the SEUS watersheds exhibit a strong rainfall elasticity meaning that there is a disproportionate response in streamflow to changes in rainfall. Similar conclusions were drawn in Schaake (1990) and Nash and Gleick (1991). From these studies, there is a growing consensus that lower elasticity is exhibited by regions where humidity and energy are seasonally out of phase (Budyko hypothesis) and in regions with a high humidity index or lower values of potential evapotranspiration.

To understand the change in the probability distribution of the rainfall due to ENSO, the rainfall for the winter season is ranked and divided in three groups of equal size: that is, lower tercile, middle tercile, and higher tercile, with each containing 33 years of data. Hence, the lower tercile corresponds to the years with lower values of rainfall, the medium tercile corresponds to the central region of the probability density of the rainfall, and so on. Subsequently, within each tercile, a



**Figure 5.** Correlation of DJF streamflow with Niño-3.4 index in (a) CRU, (b) PRISM, (c) 20CR, and (d) FLARes1.0. Positive values are shown in red and negative values are shown in blue. Statistically significant regions at the 90% level of confidence are shown as thick circles.

fraction of years featuring a particular ENSO event is calculated. A fraction of a warm or cold ENSO event in a lower or higher tercile for the four-rainfall dataset (Figure 6) shows a shift in the probability density function of rainfall. El Niño years are featured with a distribution in rainfall with a shift toward the higher ranges. Hence, events with higher values of rainfall are more frequent in El Niño years accompanied by less frequent lower values of rainfall. The opposite happens for years that feature La Niña, where we see a shift toward the lower ranges in the rainfall. This is true for all the four datasets analyzed here (CRU, 20CR, FLARes1.0, and PRISM). The neutral years and the middle tercile are not shown because they are statistically insignificant.

To verify whether such a shift also occurs in the streamflow distribution, the streamflows from the hydrological models are ranked and divided into the three tercile categories. Subsequently, the fraction of a cold and warm ENSO event in each category is analyzed (Figure 7). The results for the streamflow are in good agreement with the results of the rainfall. The direction of shift in the probability density function (PDF) of the streamflow is consistent with the shift in the distribution of rainfall for most of the watersheds in the SEUS; most importantly, they seem to be consistent across all four datasets.

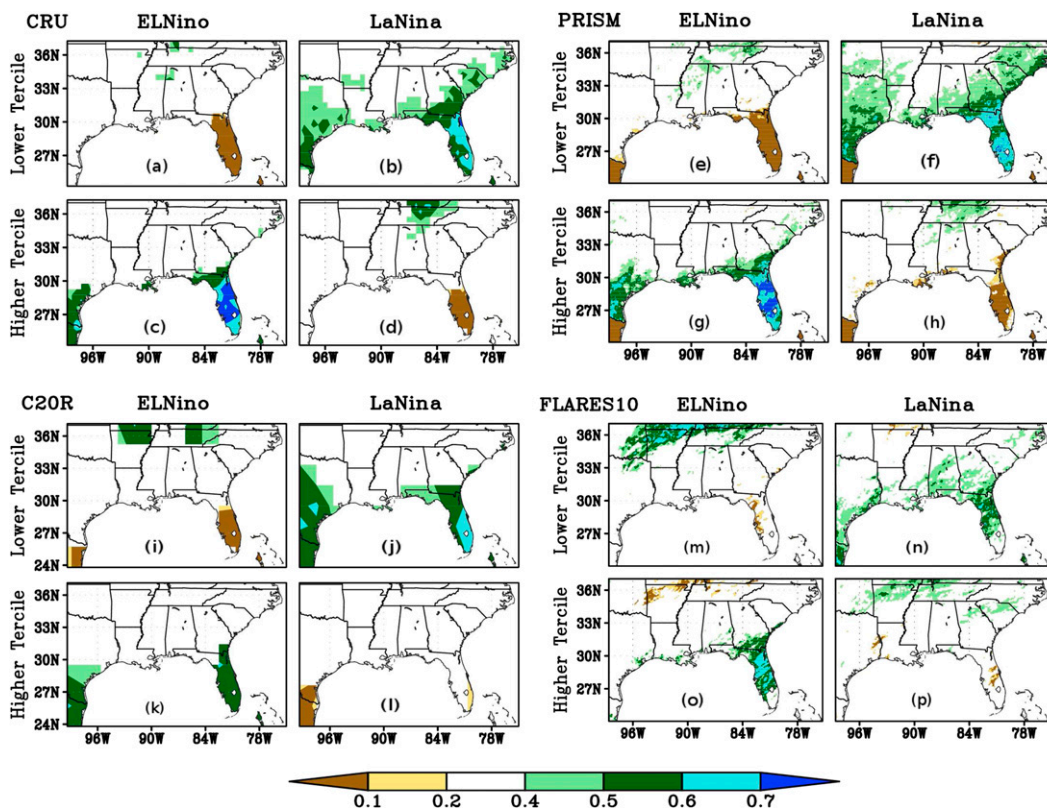
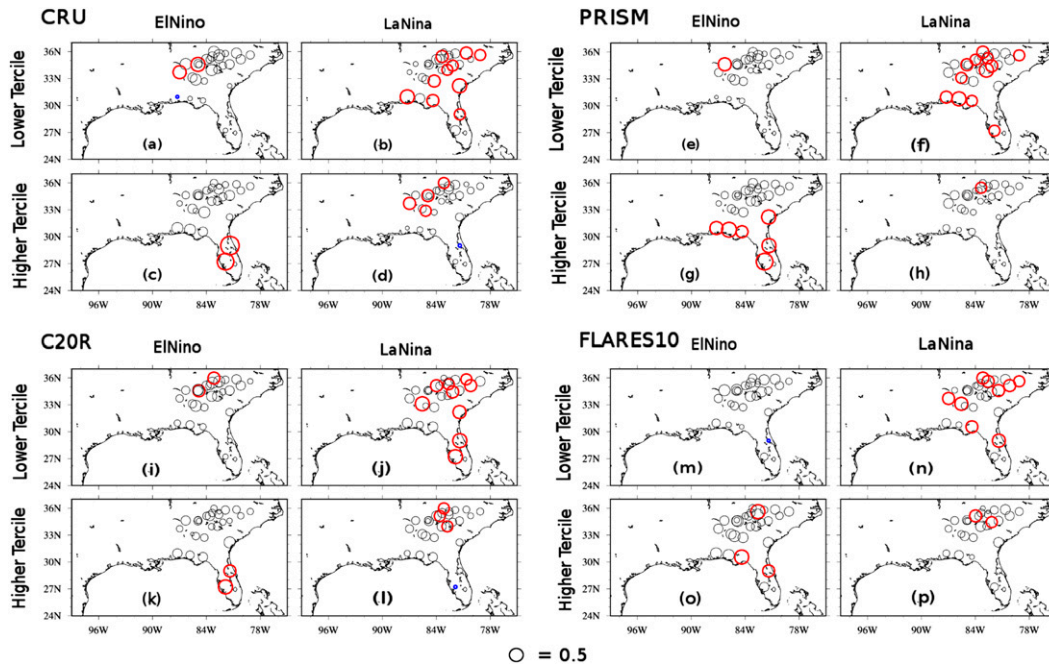


Figure 6. Fraction of warm or cold ENSO event in tercile division of precipitation for (a)–(d) CRU, (e)–(h) PRISM, (i)–(l) 20CR, and (m)–(p) FLAREs1.0. Statistically significant regions at the 90% level of confidence are shaded.

### 4.3. Interdecadal variations of the ENSO teleconnection

The AMO is a mode of sea surface temperature (SST) variability in the northern Atlantic Ocean with a period of around 60 years (Schlesinger and Ramankutty 1994). The positive phase of the AMO is chosen to be from 1930 through 1959 and the negative phase is from 1965 through 1989 (<http://www.esrl.noaa.gov/psd/data/timeseries/AMO/>). As seen in earlier works (Enfield et al. 2001; Mo 2010; Misra and DiNapoli 2012), a positive (negative) phase of the AMO suppresses (enhances) the ENSO teleconnections on the SEUS winter rainfall. In the negative phase of the AMO, the ENSO teleconnection on DJF rainfall (as depicted by the positive correlations) appears to spread slightly northward and westward of northern Florida in CRU (Figure 8a) and PRISM (Figure 8c). Furthermore, the negative correlations over Tennessee that appear during the positive phase of the AMO disappear during the negative phase of the AMO. These features of the modulated ENSO teleconnection by the AMO is broadly captured in the 20CR (Figures 8e,f) and FLAREs1.0 datasets (Figures 8g,h). In fact, the negative correlations over Tennessee during the positive phase of the AMO are well (poorly) captured in 20CR (FLAREs1.0) in Figure 8e (Figure 8g). However, the westward and



**Figure 7.** Fraction of warm or cold ENSO event in tercile division of streamflow for (a)–(d) CRU, (e)–(h) PRISM, (i)–(l) 20CR, and (m)–(p) FLAREs1.0 data. Fractions that are significantly high (>0.4) are marked in red and those that are low (<0.2) are marked in blue at the 90% level of confidence.

northward extension of the correlations during the negative phase of the AMO is reasonably well (poorly) captured in FLAREs1.0 (20CR) in [Figure 8h](#) ([Figure 8f](#)).

A similar analysis is performed on the modulation of ENSO-forced winter seasonal mean streamflow variations by the AMO. With the change from a positive phase of the AMO to the negative phase, there is a clear shift in the streamflow variability in the northern watersheds of the SEUS, which displays a stronger positive correlation in the northern watersheds to the ENSO index ([Figure 9](#)). This result is quite robust because there is a general agreement on this feature across all four climate datasets. In fact, the streamflow in some of these northern watersheds of the SEUS change their sign in their correlations with the ENSO index in moving from positive to negative phase of the AMO. This is very clearly observed in CRU ([Figures 9a,b](#)), PRISM ([Figures 9c,d](#)), and FLAREs1.0 ([Figures 9g,h](#)) but not as much in 20CR ([Figures 9e,f](#)).

On the other hand, the watersheds in south Florida show insignificant change in the ENSO teleconnections to the change in the phase of the AMO. This is consistently observed in all four climate datasets with the growing strength of the teleconnection between streamflow and ENSO index as one moves north from south Florida. Despite the lack of robust ENSO–rainfall teleconnection in the northern watersheds of the SEUS that is modulated by the AMO ([Figure 8](#)), the elasticity of the streamflows in the SEUS watersheds and the fact that the streamflow at the outlet is an aggregate response to rainfall over the entire watershed explains the appearance of the significant correlations in [Figure 9](#).

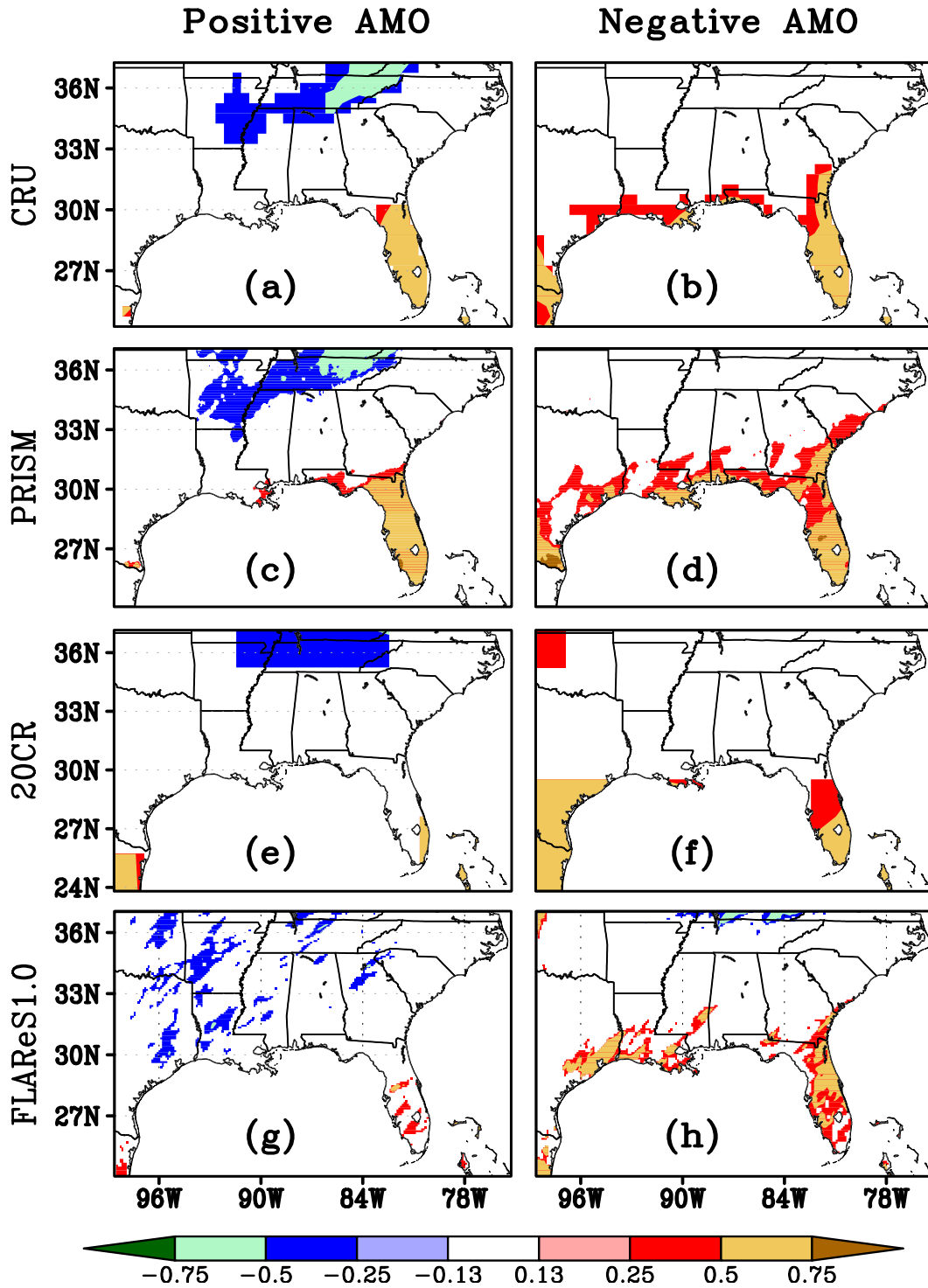
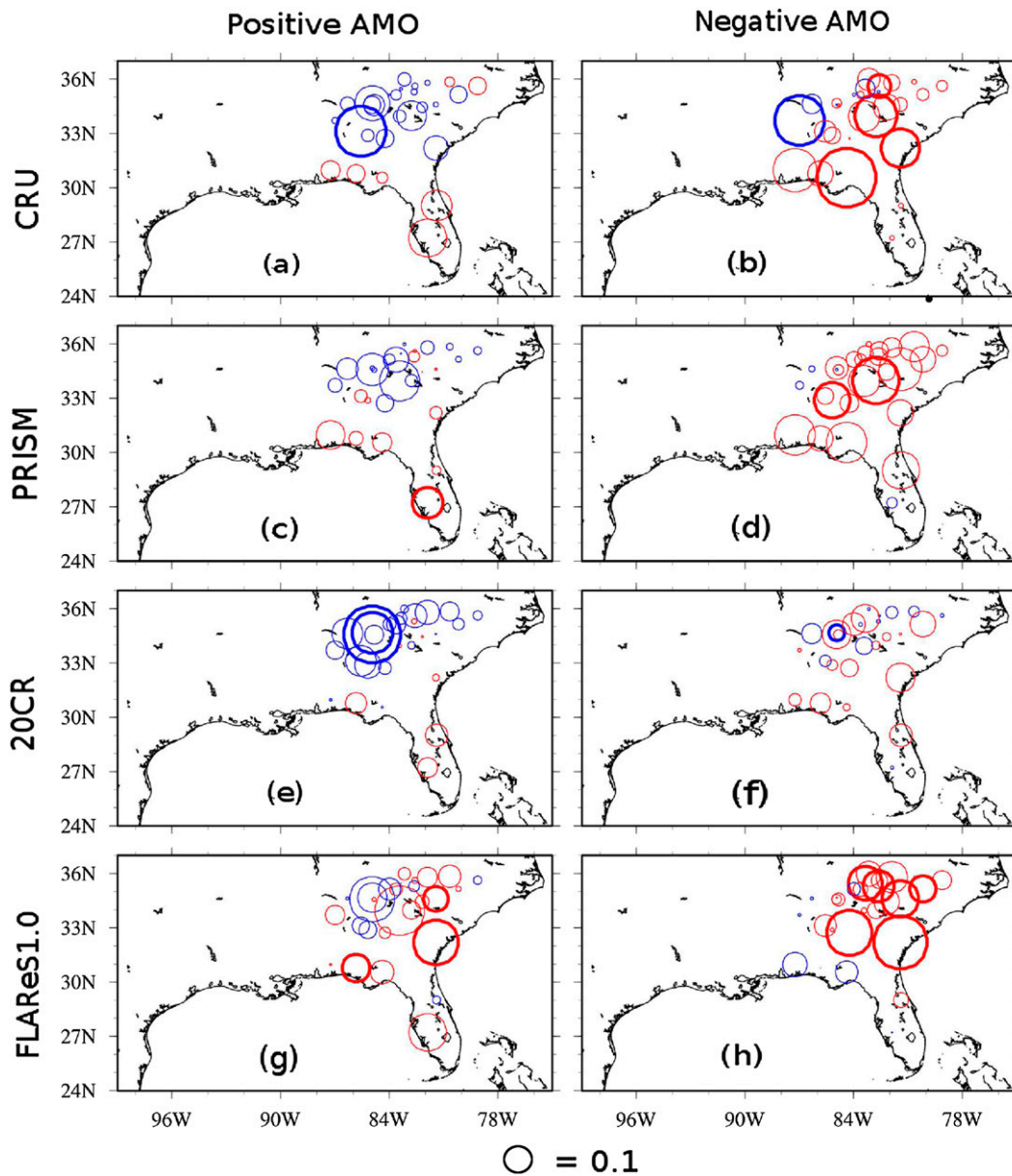


Figure 8. Correlation of DJF precipitation with the Niño-3.4 index during (a),(c),(e),(g) positive and (b),(d),(f),(h) negative phases of AMO for (a),(b) CRU, (c),(d) PRISM, (e),(f) 20CR, and (g),(h) FLARes1.0. Statistically significant regions at the 90% level of confidence are shaded.



**Figure 9.** Correlation of DJF streamflow with the Niño-3.4 index during (a),(c),(e),(g) positive and (b),(d),(f),(h) negative phases of AMO for (a),(b) CRU, (c),(d) PRISM, (e),(f) 20CR, and (g),(h) FLAREs1.0. Positive values are shown in red and negative values are shown in blue. Statistically significant regions at the 90% level of confidence are denoted as thick circles.

Furthermore, the lack of significant correlations in south Florida in [Figure 9](#) runs in contrast to [Enfield et al. \(2001\)](#), who found that, during opposite phases of the AMO, the inflow in Lake Okeechobee, which is regarded as the reservoir of the south Florida water supply, changes by as much as 40%. This study illuminates that

this variability of inflow in Lake Okeechobee forced by the AMO seems to be independent of ENSO variations in the winter. As mentioned earlier, since the watersheds of SEUS are characterized with high value of elasticity and streamflow at the basin outlet is an aggregated response to rainfall over the watershed, there is a stronger ENSO teleconnections in the streamflow in some watersheds in Alabama, Georgia, and South Carolina as compared to rainfall.

## 5. Conclusions

In this study, the association of ENSO variability with rainfall and streamflow during the boreal winter season over 28 watersheds located in the SEUS is examined across four different century-long datasets. The rainfall from the two of the four datasets is considered as observed datasets analyzed on regular grids while the other two are model generated atmospheric reanalysis. While the main objective was to intercompare the ENSO teleconnections on SEUS hydrology, a larger goal was to establish if the model generated atmospheric reanalysis could be a viable alternative to the observed rainfall datasets to discern these low-frequency variations in SEUS hydrology. An affirmative answer to the latter would help in reposing more faith in such reanalysis attempts of the SEUS hydrology.

A multimodel strategy was adopted to simulate the streamflow using rainfall from four different datasets (CRU, PRISM, 20CR, and FLAReS1.0). 20CR is the global atmospheric reanalysis at 250-km grid resolution (Compo et al. 2011). FLAReS1.0 is a dynamically downscaled atmospheric reanalysis from 20CR at 10-km grid resolution (DiNapoli and Misra 2012). The hydrological models were calibrated and validated for the period of 1949–70 using an independent set of rainfall (CPC) observations. The monthly mean rainfall datasets were disaggregated to the time step of the hydrological models (daily) using a weather generator (WGEN; Richardson and Wright 1984). Our analysis clearly indicates that the streamflow simulation errors stemming from the hydrological models are not insignificant. These errors largely stem from the erroneous forcing of the atmospheric reanalysis precipitation in comparison to rainfall from either CRU or PRISM. These errors are larger in the northern watersheds of the SEUS compared to the southern watersheds in Florida.

In this study, we have focused on ENSO teleconnections on the winter hydrology of the SEUS as it is well known to be robust and therefore an ideal metric to evaluate the fidelity of a dataset. Our analysis reveals that ENSO teleconnections with winter rainfall in the SEUS are comparable in all four datasets. The influence of ENSO variability is stronger in the southern parts of the SEUS domain compared to the northern part. This is also reflected in the ENSO teleconnections of streamflow. The variability of streamflow in the southern watersheds (over Florida) shows a stronger relationship than the northern watersheds in the SEUS. Similarly, the shift in the PDF of the intensity of rainfall and streamflow with change in ENSO phase show consistency across all four century-long datasets.

Another important feature that is analyzed in this paper is the decadal modulation of ENSO teleconnection by AMO (Enfield et al. 2001). In all four climate datasets, the winter streamflow in the northern watersheds in the SEUS show a stronger positive correlation with the ENSO index during the negative phase of

AMO. In fact, in some of these watersheds, the correlations of the winter streamflow variations with ENSO index change their sign from negative to positive correlations from positive to negative phase of AMO. These robust decadal modulations of ENSO teleconnections with streamflow in the northern watersheds of SEUS are possible despite insignificant variations of rainfall with ENSO owing to the nonlinear relationship (elasticity) between rainfall and streamflow (Sankarasubramanian et al. 2001). Furthermore, the disparity between ENSO–rainfall and ENSO–streamflow teleconnections (in Figures 8 and 9, respectively) also stems from the fact that the streamflow at watershed outlets represent the aggregate response of rainfall over the entire watershed, which happens to span a diverse region of ENSO–rainfall teleconnection in the northern regions of the SEUS. This study clearly highlights the importance of century-long datasets to resolve these important teleconnections in the SEUS.

Our study reveals that FLARes1.0 reproduced verifiable correlation of streamflow with Niño-3.4 SST index in winter, consistent shifts in the distribution of streamflow with ENSO phase and AMO modulation of ENSO effects on streamflow compared to streamflow simulated with observed gridded precipitation and larger-scale re-analysis data. However, despite this fidelity shown by FLARes1.0 forced simulated streamflow, the errors of the streamflow simulations as measured by the Nash–Sutcliffe efficiency (NSE) and volume error (VE) are discouraging. This model error shows that there is still a significant challenge in utilizing the output from climate model in reproducing the streamflow dynamics as it leads to large systematic errors. Therefore, datasets like FLARes1.0 can prove to be useful to detect the influence of large-scale climate variations on streamflows in small watersheds such as those over the SEUS, while they can still be far from adequate in simulating the streamflow dynamics of the watersheds over the SEUS at a daily time scale.

**Acknowledgments.** This work was supported by grants from NOAA (NA12OAR4310078, NA10OAR4310215, and NA11OAR4310110) and USDA (027865).

## References

- Bastola, S., and V. Misra, 2013: Sensitivity of hydrological simulations of southeastern United States watersheds to temporal aggregation of rainfall. *J. Hydrometeor.*, **14**, 1334–1344, doi:[10.1175/JHM-D-12-096.1](https://doi.org/10.1175/JHM-D-12-096.1).
- , C. Murphy, and J. Sweeney, 2011: The role of hydrological modelling uncertainties in climate change impact assessments of Irish river catchments. *Adv. Water Resour.*, **34**, 562–576, doi:[10.1016/j.advwatres.2011.01.008](https://doi.org/10.1016/j.advwatres.2011.01.008).
- Beven, K., 2005: A manifesto for the equifinality thesis. *J. Hydrol.*, **320**, 18–36, doi:[10.1016/j.jhydrol.2005.07.007](https://doi.org/10.1016/j.jhydrol.2005.07.007).
- , and A. Binley, 1992: The future of distributed models: Model calibration and uncertainty prediction. *Hydrol. Processes*, **6**, 279–298, doi:[10.1002/hyp.3360060305](https://doi.org/10.1002/hyp.3360060305).
- Boyle, D. P., H. V. Gupta, and S. Sorooshian, 2001: Multicriteria calibration of hydrologic models. *Calibration of Watershed Models*, Q. Duan et al., Eds., Water Science and Application Series, Vol. 6, Amer. Geophys. Union, 185–196.
- Cayan, D. R., K. T. Redmond, and L. G. Riddle, 1999: ENSO and hydrologic extremes in the western United States. *J. Climate*, **12**, 2881–2893, doi:[10.1175/1520-0442\(1999\)012<2881:EAHEIT>2.0.CO;2](https://doi.org/10.1175/1520-0442(1999)012<2881:EAHEIT>2.0.CO;2).

- Chiew, F. H. S., S. L. Zhou, and T. A. McMahon, 2003: Use of seasonal streamflow forecasts in water resources management. *J. Hydrol.*, **270**, 135–144, doi:[10.1016/S0022-1694\(02\)00292-5](https://doi.org/10.1016/S0022-1694(02)00292-5).
- Compo, G. P., and Coauthors, 2011: The Twentieth Century Reanalysis project. *Quart. J. Roy. Meteor. Soc.*, **137**, 1–28, doi:[10.1002/qj.776](https://doi.org/10.1002/qj.776).
- Daly, C., R. P. Neilson, and D. L. Phillips, 1994: A statistical-topographic model for mapping climatological precipitation over mountainous terrain. *J. Appl. Meteor.*, **33**, 140–158, doi:[10.1175/1520-0450\(1994\)033<0140:ASTMFM>2.0.CO;2](https://doi.org/10.1175/1520-0450(1994)033<0140:ASTMFM>2.0.CO;2).
- Dettinger, M. D., D. R. Cayan, G. M. McCabe, and J. A. Marengo, 2000: Multiscale streamflow variability associated with El Niño/Southern Oscillation. *El Niño and the Southern Oscillation—Multiscale Variability and Global and Regional Impacts*, H. F. Diaz and V. Markgraf, Eds., Cambridge University Press, 113–146.
- DiNapoli, S. M., and V. Misra, 2012: Reconstructing the 20th century high-resolution climate of the southeastern United States. *J. Geophys. Res.*, **117**, D19113, doi:[10.1029/2012JD018303](https://doi.org/10.1029/2012JD018303).
- Duan, Q., and Coauthors, 2006: Model Parameter Estimation Experiment (MOPEX): An overview of science strategy and major results from the second and third workshops. *J. Hydrol.*, **320**, 3–17, doi:[10.1016/j.jhydrol.2005.07.031](https://doi.org/10.1016/j.jhydrol.2005.07.031).
- Efron, B., and R. J. Tibshirani, 1993: *An Introduction to the Bootstrap*. Chapman and Hall, 436 pp.
- Enfield, D. B., A. M. Mestas-Núñez, and P. J. Trimble, 2001: The Atlantic multidecadal oscillation and its relation to rainfall and river flows in the continental U.S. *Geophys. Res. Lett.*, **28**, 2077–2080, doi:[10.1029/2000GL012745](https://doi.org/10.1029/2000GL012745).
- Freer, J., K. Beven, and B. Ambroise, 1996: Bayesian estimation of uncertainty in runoff prediction and the value of data: An application of the GLUE approach. *Water Resour. Res.*, **32**, 2161–2173, doi:[10.1029/95WR03723](https://doi.org/10.1029/95WR03723).
- Gershunov, A., and T. P. Barnett, 1998: Interdecadal modulation of ENSO teleconnections. *Bull. Amer. Meteor. Soc.*, **79**, 2715–2725, doi:[10.1175/1520-0477\(1998\)079<2715:IMOET>2.0.CO;2](https://doi.org/10.1175/1520-0477(1998)079<2715:IMOET>2.0.CO;2).
- Gupta, H. V., K. J. Beven, and T. Wagener, 2003: Model calibration and uncertainty estimation. *Encyclopedia of Hydrological Sciences*, M. G. Anderson, Ed., Vol. 11, John Wiley and Sons, 131, doi:[10.1002/0470848944.hsa138](https://doi.org/10.1002/0470848944.hsa138).
- Gutiérrez, F., and J. A. Dracup, 2001: An analysis of the feasibility of long-range streamflow forecasting for Colombia using El Niño–Southern Oscillation indicators. *J. Hydrol.*, **246**, 181–196, doi:[10.1016/S0022-1694\(01\)00373-0](https://doi.org/10.1016/S0022-1694(01)00373-0).
- Hidalgo, H. G., and J. A. Dracup, 2003: ENSO and PDO effects on hydroclimatic variations of the upper Colorado River basin. *J. Hydrometeorol.*, **4**, 5–23, doi:[10.1175/1525-7541\(2003\)004<0005:EAPEOH>2.0.CO;2](https://doi.org/10.1175/1525-7541(2003)004<0005:EAPEOH>2.0.CO;2).
- Higgins, R. W., W. Shi, E. Yarosh, and R. Joyce, 2000: *Improved United States Precipitation Quality Control System and Analysis*. NCEP/CPC Atlas 7, 40 pp. [Available online at [http://www.cpc.ncep.noaa.gov/research\\_papers/ncep\\_cpc\\_atlas/7/index.html](http://www.cpc.ncep.noaa.gov/research_papers/ncep_cpc_atlas/7/index.html).]
- Hughes, D. A., 2013: A review of 40 years of hydrological science and practice in southern Africa using the Pitman rainfall-runoff model. *J. Hydrol.*, **501**, 111–124, doi:[10.1016/j.jhydrol.2013.07.043](https://doi.org/10.1016/j.jhydrol.2013.07.043).
- Kanamitsu, M., K. Yoshimura, Y. B. Yhang, and S. Y. Hong, 2010: Errors of interannual variability and trend in dynamical downscaling of reanalysis. *J. Geophys. Res.*, **115**, D17115, doi:[10.1029/2009JD013511](https://doi.org/10.1029/2009JD013511).
- Kasiviswanathan, K. S., R. Cibin, K. P. Sudeer, and I. Chaubey, 2013: Constructing prediction interval for artificial neural network rainfall runoff models based on ensemble simulations. *J. Hydrol.*, **499**, 275–288, doi:[10.1016/j.jhydrol.2013.06.043](https://doi.org/10.1016/j.jhydrol.2013.06.043).
- Kiladis, G. N., and H. F. Diaz, 1989: Global climatic anomalies associated with extremes in the Southern Oscillation. *J. Climate*, **2**, 1069–1090, doi:[10.1175/1520-0442\(1989\)002<1069:GCAAWE>2.0.CO;2](https://doi.org/10.1175/1520-0442(1989)002<1069:GCAAWE>2.0.CO;2).
- Knight, J. R., C. K. Folland, and A. A. Scaife, 2006: Climate impacts of the Atlantic multidecadal oscillation. *Geophys. Res. Lett.*, **33**, L17706, doi:[10.1029/2006GL026242](https://doi.org/10.1029/2006GL026242).

- Madsen, H., 2000: Automatic calibration of a conceptual rainfall–runoff model using multiple objectives. *J. Hydrol.*, **235**, 276–288, doi:10.1016/S0022-1694(00)00279-1.
- McClave, J. T., and F. H. Dietrich II, 1994: *Statistics*. MacMillan College, 988 pp.
- Misra, V., 2007: Addressing the issue of systematic errors in a regional climate model. *J. Climate*, **20**, 801–818, doi:10.1175/JCLI4037.1.
- , and S. M. DiNapoli, 2012: Understanding the wet season variations over Florida. *Climate Dyn.*, **40**, 1361–1372, doi:10.1007/s00382-012-1382-4.
- , S. Chan, R. Wu, and E. Chassignet, 2009: Air-sea interaction over the Atlantic warm pool in the NCEP CFS. *Geophys. Res. Lett.*, **36**, L15702, doi:10.1029/2009GL038737.
- , and Coauthors, 2011: Climate scenarios: A Florida-centric view. State University System of Florida White Paper on Climate Scenarios for Florida, 71 pp. [Available online at [http://floridaclimate.org/docs/climate\\_scenario.pdf](http://floridaclimate.org/docs/climate_scenario.pdf).]
- , S. M. DiNapoli, and S. Bastola, 2013: Dynamic downscaling of the twentieth-century reanalysis over the southeastern United States. *Reg. Environ. Change*, **13** (Suppl.), 15–23, doi:10.1007/s10113-012-0372-8.
- Mitchell, T. D., and P. D. Jones, 2005: An improved method of constructing a database of monthly climate observations and associated high-resolution grids. *Int. J. Climatol.*, **25**, 693–712, doi:10.1002/joc.1181.
- Mo, K. C., 2010: Interdecadal modulation of the impact of ENSO on precipitation and temperature over the United States. *J. Climate*, **23**, 3639–3656, doi:10.1175/2010JCLI3553.1.
- Nash, L. L., and P. H. Gleick, 1991: Sensitivity of streamflow in the Colorado basin to climatic changes. *J. Hydrol.*, **125**, 221–241, doi:10.1016/0022-1694(91)90030-L.
- Oh, J., and A. Sankarasubramanian, 2012: Interannual hydroclimatic variability and its influence on winter nutrient loadings over the southeast United States. *Hydrol. Earth Syst. Sci.*, **16**, 2285–2298, doi:10.5194/hess-16-2285-2012.
- Poveda, G., A. Jaramillo, M. M. Gil, N. Quiceno, and R. I. Mantilla, 2001: Seasonally in ENSO-related precipitation, river discharges, soil moisture, and vegetation index in Colombia. *Water Resour. Res.*, **37**, 2169–2178, doi:10.1029/2000WR900395.
- Räsänen, T. A., and M. Kummu, 2012: Spatiotemporal influences of ENSO on precipitation and flood pulse in the Mekong River basin. *J. Hydrol.*, **476**, 154–168, doi:10.1016/j.jhydrol.2012.10.028.
- Refsgaard, J. C., J. P. van der Sluijs, A. L. Højberg, and P. A. Vanrolleghem, 2007: Uncertainty in the environmental modelling process—a framework and guidance. *Environ. Modell. Software*, **22**, 1543–1556, doi:10.1016/j.envsoft.2007.02.004.
- Richardson, C. W., and D. A. Wright, 1984: WGEN: A model for generating daily weather variables. USDA Agriculture Research Service Rep. ARS-8, 86 pp.
- Ropelewski, C. F., and M. S. Halpert, 1986: North American precipitation and temperature patterns associated with the El Niño/Southern Oscillation (ENSO). *Mon. Wea. Rev.*, **114**, 2352–2362, doi:10.1175/1520-0493(1986)114<2352:NAPATP>2.0.CO;2.
- , and —, 1987: Global and regional scale precipitation patterns associated with the El Niño/Southern Oscillation. *Mon. Wea. Rev.*, **115**, 1606–1626, doi:10.1175/1520-0493(1987)115<1606:GARSPP>2.0.CO;2.
- Sankarasubramanian, A., R. M. Vogel, and J. F. Limbrunner, 2001: Climate elasticity of streamflow in the United States. *Water Resour. Res.*, **37**, 1771–1781, doi:10.1029/2000WR900330.
- Schaake, J. C., 1990: From climate to flow. *Climate Change and U.S. Water Resources*, P. E. Waggoner, Ed., John Wiley, 177–206.
- , S. Cong, and Q. Duan, 2006: U.S MOPEX data set. IAHS Publ. UCRL-JRNL-221228, 25 pp. [Available online at <https://e-reports-ext.llnl.gov/pdf/333681.pdf>.]
- Schlesinger, M. E., and N. Ramankutty, 1994: An oscillation in the global climate system of period 65–70 years. *Nature*, **367**, 723–726, doi:10.1038/367723a0.

- Schmidt, N., E. K. Lipp, J. B. Rose, and M. E. Luther, 2001: ENSO influences on seasonal rainfall and river discharge in Florida. *J. Climate*, **14**, 615–628, doi:[10.1175/1520-0442\(2001\)014<0615:EIOSRA>2.0.CO;2](https://doi.org/10.1175/1520-0442(2001)014<0615:EIOSRA>2.0.CO;2).
- Smith, T. M., and R. W. Reynolds, 2004: Improved extended reconstruction of SST (1854–1997). *J. Climate*, **17**, 2466–2477, doi:[10.1175/1520-0442\(2004\)017<2466:IEROS>2.0.CO;2](https://doi.org/10.1175/1520-0442(2004)017<2466:IEROS>2.0.CO;2).
- Sugawara, M., 1995: Tank model. Computer models of watershed hydrology, V. P. Singh, Ed., Water Resources Publ., 165–214.
- Ting, M., Y. Kushnir, R. Seager, and C. Li, 2009: Forced and internal twentieth-century SST trends in the North Atlantic. *J. Climate*, **22**, 1469–1481, doi:[10.1175/2008JCLI2561.1](https://doi.org/10.1175/2008JCLI2561.1).
- Tootle, G. A., and T. C. Piechota, 2004: Suwannee River long range streamflow forecasts based on seasonal forecasts based on seasonal climate predictors. *J. Amer. Water Resour. Assoc.*, **40**, 523–532, doi:[10.1111/j.1752-1688.2004.tb01047.x](https://doi.org/10.1111/j.1752-1688.2004.tb01047.x).
- , —, and A. Singh, 2005: Coupled oceanic-atmospheric variability and US streamflow. *Water Resour. Res.*, **41**, W12408, doi:[10.1029/2005WR004381](https://doi.org/10.1029/2005WR004381).
- Wagener, T., D. P. Boyle, M. J. Lees, H. S. Wheater, H. V. Gupta, and S. Sorooshian, 2001: A framework for development and application of hydrological models. *Hydrol. Earth Syst. Sci.*, **5**, 13–26, doi:[10.5194/hess-5-13-2001](https://doi.org/10.5194/hess-5-13-2001).
- Waylen, P. R., C. N. Caviedes, and C. Juricic, 1993: El Niño-Southern Oscillation and the surface hydrology of Chile: A window on the future? *Can. Water Resour. J.*, **18**, 425–441, doi:[10.4296/cwrj1804425](https://doi.org/10.4296/cwrj1804425).
- Wilks, D. S., 1992: Adapting stochastic weather generation algorithms for climate change studies. *Climatic Change*, **22**, 67–84, doi:[10.1007/BF00143344](https://doi.org/10.1007/BF00143344).
- , and R. L. Wilby, 1999: The weather generation game: A review of stochastic weather models. *Prog. Phys. Geogr.*, **23**, 329–357, doi:[10.1177/030913339902300302](https://doi.org/10.1177/030913339902300302).
- Zorn, M. R., and P. R. Waylen, 1997: Seasonal response of mean monthly streamflow to El Niño/Southern Oscillation in north central Florida. *Prof. Geogr.*, **49**, 51–62, doi:[10.1111/0033-0124.00055](https://doi.org/10.1111/0033-0124.00055).

---

*Earth Interactions* is published jointly by the American Meteorological Society, the American Geophysical Union, and the Association of American Geographers. Permission to use figures, tables, and *brief* excerpts from this journal in scientific and educational works is hereby granted provided that the source is acknowledged. Any use of material in this journal that is determined to be “fair use” under Section 107 or that satisfies the conditions specified in Section 108 of the U.S. Copyright Law (17 USC, as revised by P.L. 94-553) does not require the publishers’ permission. For permission for any other form of copying, contact one of the copublishing societies.

---